Cement and Concrete Research 58 (2014) 131–142

Contents lists available at ScienceDirect

Cement and Concrete Research

journal homepage: http://ees.elsevier.com/CEMCON/default.asp

Amorphous silica in ultra-high performance concrete: First hour of hydration

Tina Oertel [a,b,*], Frank Hutter [a], Uta Helbig [c], Gerhard Sextl [a,d]

[a] Fraunhofer-Institute for Silicate Research ISC, Neunerplatz 2, 97082 Würzburg, Germany
[b] Chair for Inorganic Chemistry I, Universität Bayreuth, Universitätsstr. 30, 95440 Bayreuth, Germany
[c] Chair for Crystallography and X-ray Methods, Technische Hochschule Nürnberg Georg Simon Ohm, Wassertorstraße 10, 90489 Nürnberg, Germany
[d] Chair for Chemical Technology of Advanced Materials, Julius Maximilian Universität, Röntgenring 11, 97070 Würzburg, Germany

ARTICLE INFO

Article history:
Received 7 June 2013
Accepted 7 January 2014
Available online xxxx

Keywords:
Silica fume (D)
Amorphous material (B)
Hydration (A)
Cement paste (D)
Ultra-high performance concrete

ABSTRACT

Amorphous silica in the sub-micrometer size range is widely used to accelerate cement hydration. Investigations including properties of silica which differ from the specific surface area are rare. In this study, the reactivity of varying types of silica was evaluated based on their specific surface area, surface silanol group density, content of silanol groups and solubility in an alkaline suspension. Pyrogenic silica, silica fume and silica synthesized by hydrolysis and condensation of alkoxy silanes, so-called Stoeber particles, were employed. Influences of the silica within the first hour were further examined in pastes with water/cement ratios of 0.23 using in-situ X-ray diffraction, cryo scanning electron microscopy and pore solution analysis. It was shown that Stoeber particles change the composition of the pore solution. Na^+, K^+, Ca^{2+} and silicate ions seem to react to oligomers. The extent of this reaction might be highest for Stoeber particles due to their high reactivity.

1. Introduction

Ultra-high performance concrete (UHPC) was recently defined by Naaman and Wille [1] as a cement-based concrete with a compressive strength at least equal to 150 N/mm^2. This very dense and durable concrete is achieved by reducing the water/cement ratio (w/c ratio) to less than 0.3 by mass and by adding amorphous silica [2,3]. Silica fume is the most commonly used amorphous silica in cementitious systems. Its beneficial influence on concrete properties has been known since the 1950s but the topic is currently regaining considerable interest with a new focus on silica components with primary particles smaller than 100 nm, so-called nano silica. Those nano silica could further improve UHPC because of their advanced properties (e.g. higher purities, smaller primary particles and higher specific surface areas) [4].

Before the effects of silica in cementitious systems are discussed, the dissolution of silica in highly alkaline solutions needs to be considered. The chemical reactions involved are fundamental to describe the reaction mechanisms of silica components in cementitious systems. In water, the silica surface and monosilicic acid ("$Si(OH)_4$", the quotation mark refers to uncertainties about its stability) exhibit a depolymerization–polymerization equilibrium shown in Eq. (1) [5]. "$Si(OH)_4$" is only stable for low concentrations (less than $2 \cdot 10^{-3}$ M). Otherwise, "$Si(OH)_4$" and silicate ions (e.g. $H_3SiO_4^-$) condense to polysilicic acids of low molecular weight (so-called oligomeric silicate species, Eq. (2)) [5,6].

$$SiO_2(s) + 2H_2O(l) \leftrightarrow \text{"}Si(OH)_4\text{"}(aq) \quad (1)$$

$$H_3SiO_4^- + \text{"}Si(OH)_4\text{"} \rightarrow H_6Si_2O_7 + OH^- \quad (2)$$

Silicate ions ($H_3SiO_4^-$, $H_2SiO_4^{2-}$, $HSiO_4^{3-}$ and SiO_4^{4-}) are formed by deprotonation of "$Si(OH)_4$" (e.g. $H_3SiO_4^-$ according to Eq. (3)) when the pH is above 9 and by dissolution of silica (e.g. $H_3SiO_4^-$ according to Eq. (4)) when the pH rises above 10.7 [5]. Oligomerization and dissolution of silica proceed simultaneously.

$$\text{"}Si(OH)_4\text{"} + OH^- \rightarrow H_3SiO_4^- + H_2O \quad (3)$$

$$SiO_2 + OH^- + H_2O \rightarrow H_3SiO_4^- \quad (4)$$

The hydration of the Portland cement clinker minerals[1,2] (alite C_3S, belite C_2S, aluminate C_3A and aluminate ferrite C_4AF) is a complex reaction and its sub-processes are still under investigation [7]. The main processes, however, are well known [7–11]. Generally, alite hydrates and forms portlandite[1] (CH) and calcium silicate hydrate phases[1] (C–S–H

[1] Abbreviations are according to the conventional cement chemistry notation: $C = CaO$, $S = SiO_2$, $A = Al_2O_3$, $F = Fe_2O_3$, $H = H_2O$ and $S = SO_3$.
[2] Alite, belite, aluminate and aluminate ferrite contain impurities. Therefore their chemical composition is slightly different than the composition of the pure minerals C_3S, C_2S, C_3A and C_4AF.

* Corresponding author. Tel.: +49 911 5880 1247; fax: +49 911 5880 5177.
E-mail addresses: tina.oertel@isc.fraunhofer.de (T. Oertel), uta.helbig@th-nuernberg.de (U. Helbig).

0008-8846/$ – see front matter © 2014 Elsevier Ltd. All rights reserved.
http://dx.doi.org/10.1016/j.cemconres.2014.01.008

phases, $C_3S_2H_4$, $C_xS_uH_{w+x}$). This chemical reaction is approximately represented by Eq. (5) [10,12].

$$2C_3S + 7H \rightarrow C_3S_2H_4 + 3CH \quad (5)$$

Thereby, alite ($C_3S = 3CaO \cdot SiO_2$) dissolves congruently (Eq. (6)) in the first seconds after mixing with water to ionic species [7].

$$3CaO \cdot SiO_2 + 3H_2O \rightarrow 3Ca^{2+} + H_2SiO_4^{2-} + 4OH^- \quad (6)$$

Besides alite, the aluminate phase determines early processes. It reacts with calcium sulfate[1] ($C\bar{S}H_2$) to ettringite[1] ($C_6A\bar{S}_3H_{32}$, Eq. (7)) [9,10] which is formed to a certain amount quickly after the addition of water [13–15].

$$C_3A + 3C\bar{S}H_2 + 26H \rightarrow C_6A\bar{S}_3H_{32} \quad (7)$$

The effects of silica in cementitious systems were most often studied for so-called ordinary concretes (OC), i.e. for concretes with compressive strengths lower than approx. 60 N/mm^2 and w/c ratios higher than 0.35 by mass [16–21]. The beneficial contribution of silica in those concretes is twofold. On the one hand, *C–S–H* phases are formed in the pozzolanic reaction with portlandite (Eq. (8)) which results from the hydration of alite (Eq. (5)).

$$uS + xCH + wH \rightarrow C_xS_uH_{w+x} \quad (8)$$

On the other hand, silica particles fill voids between particles of cement and other components because they are significantly smaller (so-called filler effect) [8]. The prerequisite for an optimal effect is the dispersion to primary particles [22]. The filler effect supports the formation of a denser microstructure because the gaps between the particles are minimized which have to be bridged by hydration products [23]. Furthermore, *C–S–H* phases from alite hydration nucleate on the silica surface [18,24]. This process is also attributed to the filler effect but is more precisely called the seeding effect.

It is commonly observed and accepted that the addition of silica accelerates the cement hydration [16–20,25–28], but the exact mechanism is not yet known and different models are proposed. The acceleration is generally attributed to the seeding effect because the hydration proceeds faster in the presence of nucleation sites for *C–S–H* phases [29]. Some others conclude that silica cannot dissolve because the concentration of silicate ions would increase and subsequently suppress the hydration of alite [16]. On the contrary, other authors [17,25,26,30] postulate that silica dissolves rapidly in the pore solution of concrete (Eq. (4)) prior to the pozzolanic reaction (Eq. (8)). They propose that the pozzolanic reaction reduces the concentrations of Ca^{2+} and OH^- ions and therefore the dissolution of alite would be accelerated [17,25,26,30].

The discussion is further complicated because differing properties of different types of silica may affect the reaction mechanism. The specific surface area was identified as the most important factor [16,17,26,27,30]. Some authors further assume that the content of ≡Si – OH groups (so-called silanol groups) is also of crucial importance [16,25,31]. The silanol group density depends on the conditions during the synthesis of the silica. Although silanol groups form during the synthesis at high temperatures (e.g. the flame hydrolysis of $SiCl_4$), a considerable amount of those groups condenses to ≡Si – O – Si – bonds (so-called siloxane bonds) and aggregates of individual particles are formed when silanol groups of adjacent particles condense [5,32]. Otherwise, a considerably higher amount of silanol groups remains after the hydrolysis and condensation of alkoxy silanes at ambient temperatures (e.g. using the Stoeber process [33]) [34]. In detail, a certain amount of surface ethoxy groups (≡Si – O – C_2H_5) does not condense throughout the Stoeber process. They are subsequently replaced by silanol groups in an aqueous medium [34,35]. One might expect that the silanol group density has an influence on the silica reactivity because silanol groups adsorb ions, water and other polar molecules [36]. If a surface consists mostly of siloxane bonds, it is considered to be hydrophobic because of the lower concentration of adsorption sites [36].

Two mechanisms were proposed so far to describe the acceleration of the cement hydration when the amount of silanol groups is increased. On the one hand, Björnström et al. [16] suggest that silicate ions from the dissolution of alite (Eq. (6)) preferentially react with those groups. On the other hand, Mostafa and Brown [31] and Qing et al. [25] assume that silanol groups react with portlandite to *C–S–H* phases (Eq. (8)). Besides [16,25,31], there are only a few studies which distinguished between different types of silica (e. g. silica from flame hydrolysis or silica prepared by the Stoeber process) and their particular influence on cement hydration.

The described observations were mostly made on OC, but it is of interest to investigate how well the results may be transferred to UHPC. In the literature described so far, only Qing et al. [25] and Korpa et al. [26,28] used w/c ratios less than 0.3 by mass which are suitable for UHPC. The major difference between both cementitious systems is that the clinker minerals fully hydrate in OC (approximately a w/c ratio of 0.38 by mass is necessary [8]), whereas the amount of water is insufficient for a complete hydration in UHPC. Subsequently, less portlandite is available in UHPC for the pozzolanic reaction of silica in comparison to OC.

The aim of this study is to further investigate if certain silica properties have an influence on the early hydration of UHPC and if there is a prevalent reaction mechanism. Three different silica components are used: conventional silica fume, commercial pyrogenic silica and Stoeber particles synthesized by hydrolyzing alkoxy silanes. They are characterized for their specific surface areas, silanol group densities and solubilities in alkaline suspension. Based on the results, their hypothetical reactivities in a cementitious environment are evaluated. Further effects are investigated directly in the mixtures of cement, silica and water (so-called pastes) with very low w/c ratios (suitable for UHPC) by in-situ X-ray diffraction (XRD), cryo scanning electron microscopy (cryo SEM) and pore solution analysis.

2. Experimental procedures

2.1. Materials

The following types of silica were used: silica fume (Silicoll P®, undensified, Sika GmbH, Germany), pyrogenic silica (AEROSIL® OX 50, Evonik Industries, Germany) and Stoeber particles (prepared at Fraunhofer-Institute ISC).

Silica fume and pyrogenic silica are formed in high temperature processes: pyrogenic silica in a flame hydrolysis reaction of silicon tetrachloride at about 1800 °C (Eq. (9)) [37,38] and silica fume as a by-product of the industrial silicon production through oxidization of gaseous SiO at temperatures above 2000 °C (Eq. (10)) [8,38,39].

$$SiCl_4 + 2H_2 + O_2 \rightarrow SiO_2 + 4HCl \quad (9)$$

$$2SiO + O_2 \rightarrow 2SiO_2 \quad (10)$$

The suspension of Stoeber particles was synthesized by hydrolysis and condensation of tetraethyl orthosilicate ($Si(OC_2H_5)_4$) to amorphous silica particles in an ethanolic (C_2H_5OH) solution with ammonia (NH_3) catalysis (Eq. (11)) [33]. 6750.0 g of C_2H_5OH (CSC Jäckle Chemie GmbH, Germany), 337.5 g of aqueous NH_3 solution (25%, Sigma-Aldrich Chemie GmbH, Germany), 337.5 g of $Si(OC_2H_5)_4$ (98%, Sigma-Aldrich Chemie GmbH, Germany) and 281.3 g of de-ionized water were mixed in a round-bottom flask and rested for 24 h at room temperature. The mean particle size of 242 nm was adjusted by the relative concentrations of precursors ($Si(OC_2H_5)_4$, H_2O) and catalyst (NH_3). After synthesis, C_2H_5OH and NH_3 were stepwise exchanged with de-ionized water by rotary evaporation. This exchange is sufficient to replace surface ethoxy groups with silanol groups [35] and to remove adsorbed NH_4^+ ions from the silica surface (confirmed by infrared spectroscopy

and X-ray photoelectron spectroscopy, data not shown). The aqueous suspension was concentrated to 50 wt.% by further rotary evaporation. The temperature was maintained below 40 °C during the whole process.

$$Si(OC_2H_5)_4 + 2H_2O \rightarrow SiO_2 + 4C_2H_5OH \quad (11)$$

The Portland cement CEM I 52.5R HS/NA (high initial strength R, high sulfate resistance HS, low alkali content NA; Holcim Sulfo 5, Holcim AG, Germany) was used with the following composition of clinker minerals and contents of alkalis and sulfates in wt.%: C_3S 64.6, C_2S 12.8, C_3A 0.2, C_4AF 16.6, K_2O 0.39, Na_2O 0.48 and SO_3 2.19 (provided by the supplier).

Polycarboxylate ether (SikaViscoCrete®-2810, Sika GmbH, Germany) was applied as superplasticizer. Its water content (60 wt.%) was considered in the calculation of the w/c ratio.

2.2. Preparation of pastes

The applied paste formulation (Table 1) was based on the UHPC formulation M3Q developed by Fröhlich and Schmidt [40]. The w/c ratio was 0.23 by mass. Silica fume, pyrogenic silica or Stoeber particles were used as silica component. These pastes are further referred to as UHPC pastes.

Powderous silica (silica fume and pyrogenic silica) was premixed with cement by a handheld kitchen mixer (1 min). The superplasticizer was dissolved in de-ionized water. Then, the UHPC pastes were prepared by mixing the powder blend with the solution of superplasticizer and water. As soon as the pastes had liquefied, they were further mixed for 4 min.

For UHPC pastes with the Stoeber particle suspension, the superplasticizer was first homogenized with the cement in a grinding dish to a powder and subsequently mixed with the aqueous silica suspension (50 wt.% according to M3Q) using the kitchen mixer (4 min). This modification was necessary because attempts to dissolve the superplasticizer in the silica suspension led to a gelation of the silica particles.

2.3. Characterization methods

Silica particles were imaged by scanning electron microscopy (SEM; Carl Zeiss Supra 25). The specific surface area was measured by nitrogen adsorption (BET method; Quantachrome Autosorb 3B) after drying of the sample for 16 h at 110 °C and 10^{-6} bar. Further characterization was done by X-ray fluorescence spectroscopy (XRF; PANalytical Axios-Advanced) and X-ray diffraction (XRD; Philips PW 1710).

Stoeber particles for investigation by ^{29}Si magic angle spinning solid-state NMR spectroscopy (^{29}Si MAS NMR; Bruker Avance 500) were freeze-dried from the suspension to minimize the influence of the drying procedure on the silica surface. Pyrogenic silica and silica fume were measured as received. The quantification of the relative amounts of Q^n groups (n = 1, 2, 3 and 4) is based on a Gaussian fit of the spectrum (spinning rate = 7000 Hz).

In the Sears titration [41], the amount of sodium hydroxide (NaOH) was measured which increases the pH of an aqueous silica suspension from 4.0 to 9.0. 1.5 g silica, 100 ml de-ionized water and 30 g NaCl were mixed in a beaker and acidified with 0.1 M HCl to pH 4.0. The specific surface area was calculated from the amount of consumed NaOH using Sears' assumption that 1.26 silanol groups per nm^2 are deprotonated at the silica surface between pH 4.0 and pH 9.0. Sears based his assumption on titration studies with colloidal silica prepared by ion exchange in dilute solutions of sodium silicate. Detailed experimental procedures and the empiric equation are given in Sears [41].

Dynamic light scattering (DLS) was carried out using a Malvern Zetasizer Nano-ZS ZEN3600 device (polystyrene cuvettes, measured undisturbed, 25 °C) to determine the particle size of silica in aqueous suspensions and to monitor the dissolution process (further information in Section 2.4).

Samples of UHPC paste were investigated by in-situ XRD recorded with a PANalytical X'Pert Pro diffractometer using Cu Kα radiation. A secondary nickel filter was used to suppress fluorescence. Samples were transferred to the sample holder immediately after mixing; the surface was smoothed and sealed with a Kapton® polyimide foil to prevent evaporation of water. Measurements were taken with an X'Celerator detector (counting time 21 s) 10 min and 1 h after mixing.

The UHPC pastes for cryo SEM imaging (Carl Zeiss Leo 1530VP SEM, field emission gun; Gatan Alto 2500 cryotransfer unit) were shock frozen in liquid nitrogen (−196 °C) to stop the hydration after 1 h (at 100% r. humidity, 20 °C). Frozen samples were transferred to the SEM and a brittle fracture was introduced with a micromanipulator. The frozen water was sublimated (20 kV, 2.0 mbar) for 6 min–7 min to uncover the surface. Subsequently, the samples were sputtered with Au/Pd. Details on this sample preparation are given elsewhere [42,43].

Inductively coupled plasma optical emission spectroscopy (ICP-OES; Agilent Technologies ICP-OES Vista Pro Radial) was used to measure the chemical composition of the pore solution which was obtained from the UHPC pastes by a two-step centrifugation. Pore solution was first separated from the paste by centrifugation for 5 min (Hermle Z513K large volume centrifuge, 5000 rpm). Then, the supernatant was collected with a pipette and centrifuged for 90 min to separate silica particles and nano scale reaction products (Eppendorf Microcentrifuge 5415R, 13,200 rpm). The pH value of the pore solutions was measured with an electrode (WTW microprocessor pH meter 535) for UHPC pastes with silica fume and pyrogenic silica. Indicator paper (pH range 11.0–13.0) had to be applied for UHPC pastes with Stoeber particles because the amount of retained pore solution was too little to be measured with an electrode.

2.4. Procedure for dissolution test

The dissolution behavior of silica in a highly alkaline suspension (pH = 13.5) was recorded time dependently by determining the mean particle size with DLS. Silica suspensions for DLS measurements (5 wt.%) were prepared either by dilution of Stoeber suspensions with de-ionized water or by dispersing silica powders (pyrogenic silica or silica fume) in de-ionized water with an ultrasonic wand (Branson Sonifier 450). The silica suspensions were treated in an ultrasonic bath for 5 min and afterwards they were diluted with KOH solution (0.5 M, Merck, Germany) to 0.3 wt.%. The measurements started 1 min after contact of KOH solution and silica suspension. The silica suspensions were monitored until all particles were dissolved (termination criterion: count rate < 1 count per second) or up to 24 h. As a reference, suspensions in de-ionized water (solid content 0.3 wt.%) were measured in the same manner.

Table 1
Composition of UHPC paste based on M3Q [40] with w/c = 0.23 by mass.

Material	Density [g/cm^3]	Content per volume [kg/m^3]
Water	1.0	175.0
Portland cement	3.0	825.0
Silica	2.2	175.0
Superplasticizer	1.1	27.5

3. Results and discussion

3.1. Characterization of silica

Stoeber particles, silica fume and pyrogenic silica have spherical primary particles differing in size and size distribution which is apparent from SEM images of the dried material (Fig. 1 and Table 2) and DLS measurements of the aqueous suspensions (Fig. 2). The size of Stoeber particles in an aqueous suspension (determined by DLS, d_{50} = 242 nm) is comparable to observations from dried powders (SEM imaging,

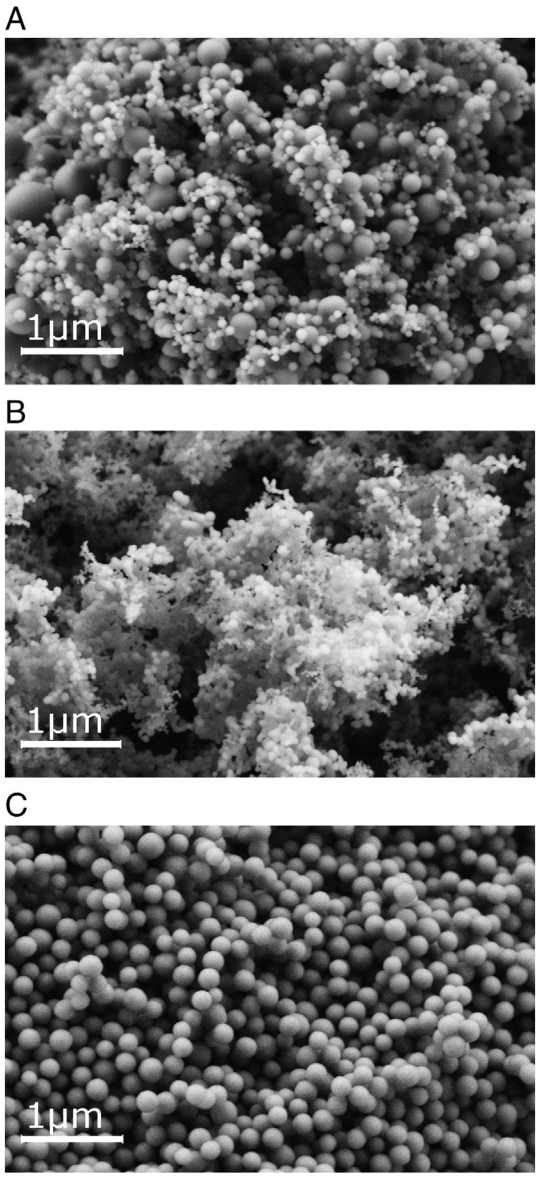

Fig. 1. SEM image of A) silica fume, B) pyrogenic silica and C) Stoeber particles. Stoeber particles show the narrowest particle size distribution.

200–250 nm). This result indicates that Stoeber particles are dispersed to primary particles in the aqueous suspensions [22]. In contrast, silica fume and pyrogenic silica are dispersed only to aggregates of their primary particles because the derived hydrodynamic diameter in aqueous suspensions differs from the primary particle size determined from SEM images. This result is consistent to former observations [5,22,32,44,45].

The specific surface area (BET method) is in the same range for silica fume and Stoeber particles, whereas it is almost twice as high for pyrogenic silica (Table 2).

Table 2
Primary particle size, specific surface areas and surface silanol group density of silica.

		Silica fume	Pyrogenic silica	Stoeber particles
Primary particle size (SEM images)	nm	30–420	35–110	200–250
Specific surface area (BET method)	m^2/g	20	38	17
Specific surface area (Sears titration)	m^2/g	11	41	(603)[a]
Surface silanol group density [41] (pH = 9.0)	nm^{-2}	<1.26	≈1.26	≫1.26

[a] Unreasonable high value because Sears' assumption is not valid (see Section 3.1).

Stoeber particles and pyrogenic silica (SiO_2 = 99.97 wt.%, determined by XRF) have a higher purity than silica fume (SiO_2 = 98.58 wt.%) [22].

The XRD pattern of pyrogenic silica (Fig. 3) is typical for amorphous silica with the broad peak at a d-value of approx. 4 Å and it is similar to patterns of silica fume and Stoeber particles [22]. Additional weak peaks were observed for silica fume in a previous study [22] which correspond to SiC.

The content of differently bound Si atoms (Q^1, Q^2, Q^3 and Q^4) can be judged by ^{29}Si MAS NMR spectroscopy (Fig. 4). Q^3 symbolizes a Si atom bound to one terminating oxygen atom and three siloxane bonds ($(\equiv Si-O)_3Si-O^-$) and corresponds e.g. to a single silanol group. Stoeber particles have the highest content of Q^3 and Q^2 groups (referring to single and geminal silanol groups) which is more than 3 times higher than for pyrogenic silica and more than 5 times higher than for silica fume. Moreover, pyrogenic silica has slightly more single silanol groups than silica fume.

Estimations on the surface silanol group density can be made by comparing specific surface areas determined by BET method and by Sears titration (Table 2). In the Sears titration, it is assumed that 1.26 silanol groups per nm^2 are deprotonated on the silica surface between pH 4.0 and pH 9.0 [41]. The deprotonation of a single silanol group is shown in Eq. (12) [5].

$$\equiv Si-OH + OH^- \rightarrow \equiv Si-O^- + H_2O \quad (12)$$

The specific surface areas determined by BET method and by Sears titration fit well for pyrogenic silica which indicates a surface silanol group density similar to Sears' assumption of 1.26 nm^{-2}. For the other silica, specific surface areas obtained from the BET method differ from those derived from the Sears titration. Therefore, the surface silanol group density of silica fume is expected to be lower than the assumed 1.26 nm^{-2} and of Stoeber particles significantly higher than this value.

When evaluating the titration of Stoeber particles, it needs to be considered that a certain amount of internal silanol groups might be deprotonated by NaOH because OH^- ions enter through micropores [46,47]. It was concluded from several authors [47–49] that Stoeber particles possess a microporosity not being detected by the BET method because the pores, although being penetrated by OH^- ions, are impermeable to nitrogen [47,48] or only exist in an aqueous environment [50]. The later was investigated by Yates and Healy [50] arguing that a gel layer of polysilicic acid surrounds the silica particles which forms when the amount of surface silanol groups is sufficient. It was further proposed that the pores only exist in aqueous suspension and are compacted during drying the samples in preparation for the BET method [50].

The results concerning the surface silanol group density presented in this study correspond to former observations where the surface silanol group density of pyrogenic silica was determined to 2–3 nm^{-2} [5,32] and of Stoeber particles to approx. 4.9 nm^{-2} [35]. Moreover, they are consistent with the total content of silanol groups determined by ^{29}Si MAS NMR spectroscopy which include surface and internal silanol groups.

The dispersabilities, contents of silanol groups and surface silanol group densities are in accordance with the conditions of formation of the silica (Section 2.1). It was stated in the Introduction that a high amount of silanol groups remains after the synthesis of discrete Stoeber particles at ambient temperatures [34], whereas a considerable amount of those groups condenses in the flame hydrolysis of pyrogenic silica and aggregates of individual particles are formed [5,32]. Silica fume is formed at water-free conditions [38]. Therefore, silanol groups might only be formed after the synthesis through hydroxylation with liquid or vaporous water [34,51]. Moreover, aggregates of primary particles are rapidly build up during the formation of silica fume at high temperatures.

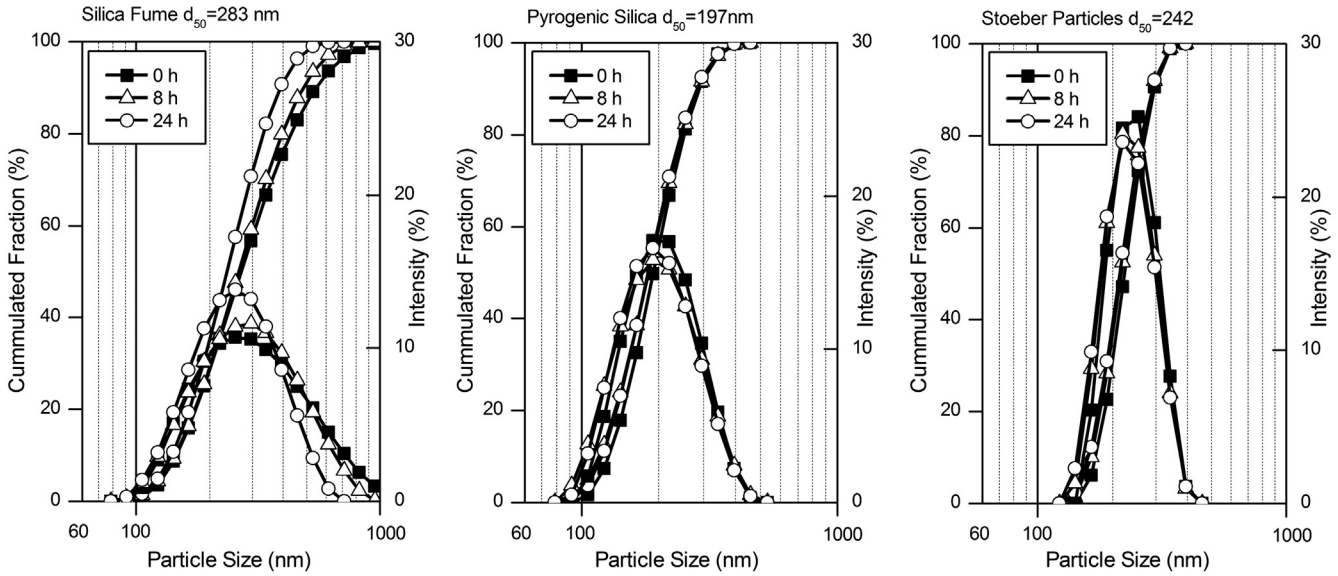

Fig. 2. Particle size distribution and mean particle size (d_{50}) of silica fume, pyrogenic silica and Stoeber particles in de-ionized water measured by DLS throughout 24 h (hydrodynamic diameter, 0.3 wt.% solid content, values after 4 min, 8 h and 24 h are shown). The particle size distribution shifts to smaller values for silica fume.

3.2. Solubility of silica in highly alkaline medium

The dissolution of silica in an aqueous dispersion of 0.5 M KOH and in de-ionized water (reference values) was observed by determining the particle sizes via DLS during 24 h (Fig. 5). The dissolution is indicated by a decreasing mean particle size and the shift of the particle size distribution to smaller particles (Fig. 6). The starting concentration of silica particles was 0.3 wt.%. It should be considered that the measured particle sizes of Stoeber particles refer to their primary particles whereas those of pyrogenic silica and silica fume to aggregates (Section 3.1).

For silica fume dispersed in de-ionized water, the mean aggregate size decreases somewhat (Fig. 5) and the aggregate size distribution shifts slightly to smaller particles (Fig. 2). Initially, 5 vol.% of aggregates are larger than 600 nm. After 24 h, only a minor amount of large particles remains which shows that aggregates of silica fume settle within the observation period of 24 h. The mean size and the size distribution for Stoeber particles and aggregates of pyrogenic silica remain constant in de-ionized water which indicates stable suspensions. Consequently, a significant decrease of the mean particle/aggregate size for measurements in aqueous dispersions of KOH is a reliable indicator for the dissolution of particles/aggregates.

Dispersed in aqueous solutions of KOH, Stoeber particles are dissolved completely after around 1.5 h, whereas aggregates of pyrogenic silica dissolve slowly and are still present after 24 h (Fig. 5 and 6). The correlation of the results with the specific surface areas of the silica samples shows that the dissolution of silica must also be dependent on other characteristics of the material. In detail, the specific surface area of pyrogenic silica is twice as high as of Stoeber particles but the dissolution rate is significantly lower. The faster dissolution of Stoeber particles is attributed to the higher amount of silanol groups and the lower amount of siloxane bonds (Section 3.1) because silica dissolution is rate controlled by breaking the strong siloxane bonds through hydrolysis [52]. Therefore, the dissolution rate of silica increases with an increasing initial amount of silanol groups [53,54] depending strongly on the conditions of formation as was previously discussed in Section 3.1. In conclusion, pyrogenic silica dissolves more slowly than Stoeber particles

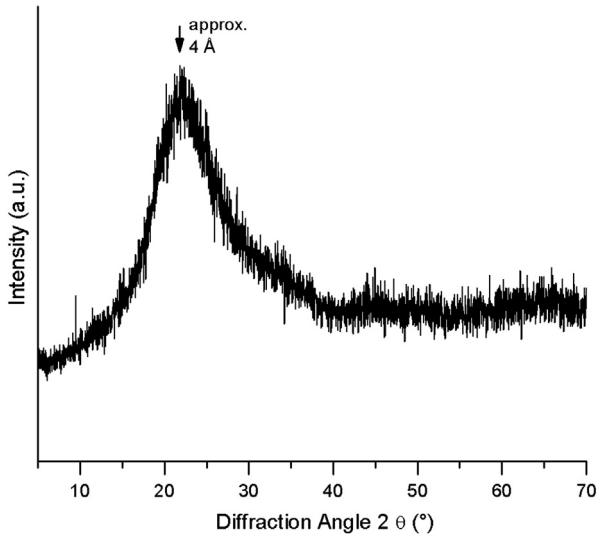

Fig. 3. X-ray diffraction pattern of pyrogenic silica. The broad peak at approx. d = 4 Å is the amorphous hump.

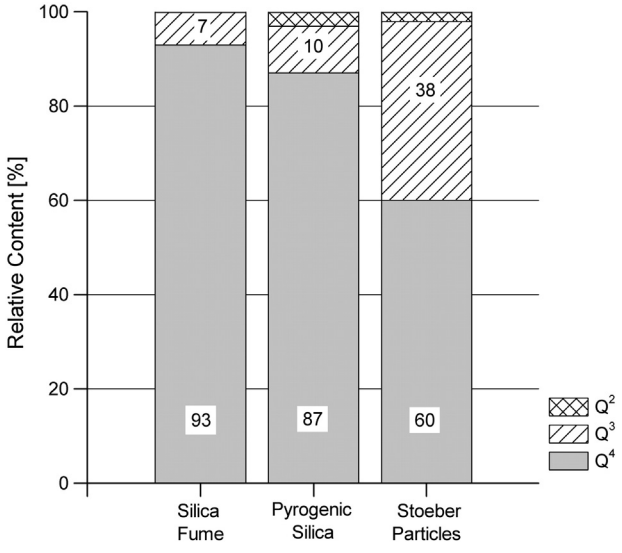

Fig. 4. Quantification of Q^{2-4} groups based on the integration of Gaussian fit of ^{29}Si MAS NMR spectra (spinning rate = 7000 Hz). Stoeber particles have the highest amount of Q^3 groups.

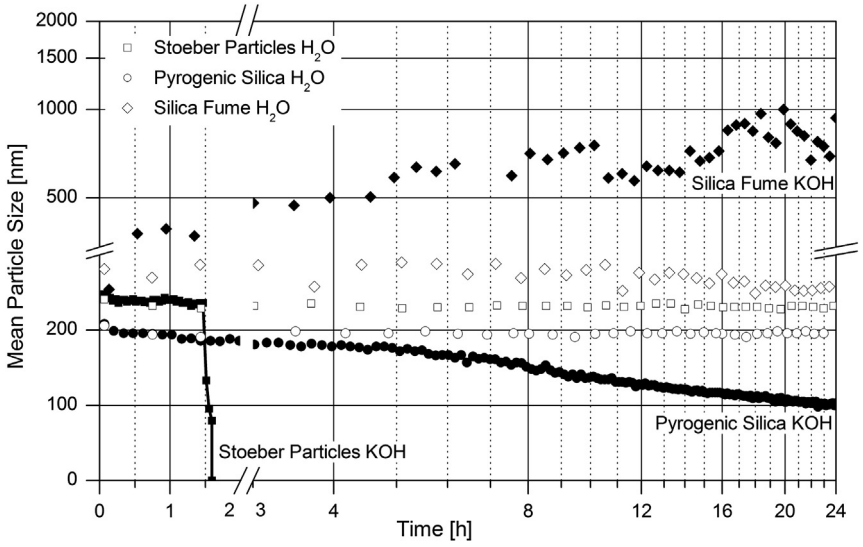

Fig. 5. Mean particle size of silica fume, pyrogenic silica and Stoeber particles in aqueous dispersion of 0.5 M KOH (pH = 13.5) and in de-ionized water measured by DLS throughout 24 h (0.3 wt.% solids content). The particle size decreases quickly for Stoeber particles and slowly for pyrogenic silica. The particle size of silica fume increases significantly.

because of its lower surface silanol group density and low total content of silanol groups.

The dissolution behavior of silica fume could not be observed via DLS. The aggregates coagulate very rapidly in KOH to clusters (approx. 5 μm, data not shown). They are too large to be measured by DLS commonly employed in the range of 0.002–2 μm [55]. The size of remaining clusters can be determined after filtering the suspension with a 0.45 μm syringe filter 1 min after its preparation (Figs. 5 and 6). The results give evidence that the coagulation proceeds throughout the measurement because the particle size increases. The noisy data after approx. 10 h might be explained by a simultaneous settling of large agglomerates formed by coagulation. Both, coagulation and settling, make it difficult to detect the dissolution of particles in this experiment. However, it is suggested that silica fume dissolves more slowly than pyrogenic silica because it has a lower silanol group density, a lower total content of silanol groups and a smaller specific surface area (Section 3.1).

An explanation for the different coagulation behavior might be given by the Derjaguin–Landau–Verwey–Overbeek theory (DLVO theory). It describes the interaction of approaching particles of almost all oxide colloidal materials by a potential originating from attractive van der Waals forces and repulsive electrostatic forces [56–58]. The stability of silica particles towards coagulation is strongly dependent on the negative surface charge which results from the deprotonation of silanol groups through OH^- (Eq. (12)) [5]. Charge neutrality between the silica particles and the aqueous medium is maintained by the adsorption of counter ions (K^+ in this experiment) and co-ions (OH^- in this experiment) which form the so-called double layer. The repulsive electrostatic forces originate from the overlap of the electric double layers of approaching particles [59]. One can conclude that sufficiently high surface charges prevent a coagulation of silica fume, pyrogenic silica and Stoeber particles in de-ionized water (reference values).

The DLVO theory further explains the influence of the ionic strength of the dispersion medium. The ionic strength of the KOH solution reduces the thickness of the electric double layer of the particles in comparison to those in de-ionized water [59]. This compression of the double layer decreases the electrostatic repulsive force. In consequence, if the repulsive force is too low, the distance of the particles becomes small enough that van der Waals attraction promotes the coagulation of particles [59]. Besides the ionic strength, the particle size has a significant influence on the electrostatic repulsive force. The thickness of the

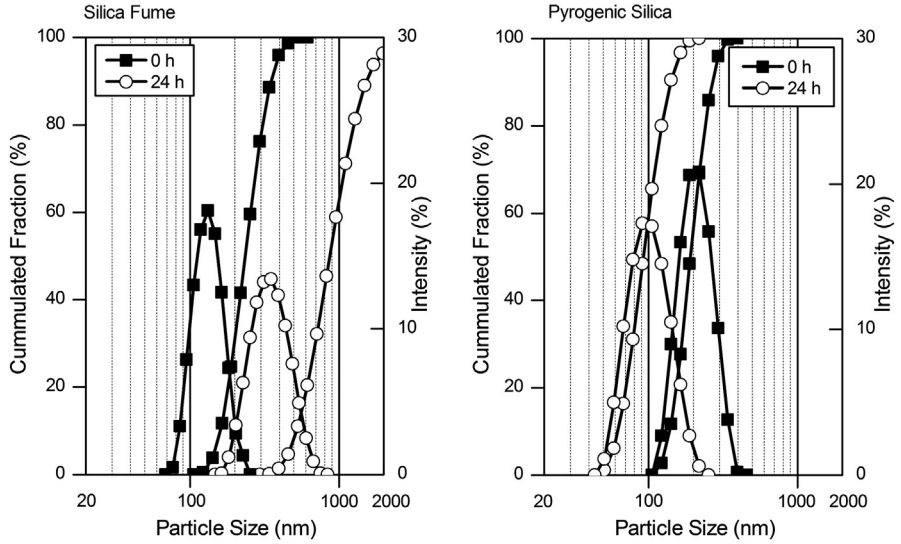

Fig. 6. Particle size distribution of silica fume and pyrogenic silica in 0.5 M KOH measured by DLS throughout 24 h (hydrodynamic diameter, pH = 13.5, 0.3 wt.% solid content, values after 4 min and 24 h are shown). The particle size distribution increases for silica fume, whereas it declines for pyrogenic silica.

double layer is independent of the particle size. Subsequently, the ratio of particle size to thickness of the electric double layer decreases with an increasing particle size and the electrostatic repulsive force is reduced. According to the results of this experiment, the repulsive forces seem to be large enough for Stoeber particles and pyrogenic silica to prevent the coagulation of particles in KOH suspensions; however, they are too low for particles of silica fume which subsequently coagulate.

Although silica particles dissolve under the given conditions in the KOH solution and therefore their coagulation behavior might not completely conform to the DLVO theory, the described size dependency of the coagulation is in accordance to the observation that Stoeber particles with a size of 740 nm coagulate in KOH suspensions (procedure similar to Section 2.4, data not shown). Therefore, it is concluded that aggregates of silica fume (283 nm) might be too large to be stabilized towards coagulation, whereas Stoeber particles (242 nm) and aggregates of pyrogenic silica (197 nm) seem to be too small to coagulate under the given conditions.

Apart from the DLVO theory, some authors [50,60] propose that stabilizing layers other than the double layer determine the stability of silica particles in aqueous suspensions. Jenkins et al. [60] suggest that the repulsion of particles is enhanced with an increasing amount of deprotonated silanol groups on the silica surface. These silanol groups attract solvated counter ions forming a layer around the silica particles. The gel layer of polysilicic acid suggested by Yates and Healy [50] (previously described in Section 3.1) is also strongly related to the amount of surface silanol groups. The conclusion can be drawn for both layers that agglomerates of silica fume should have the lowest stability towards coagulation in alkaline media because they have the lowest amount of silanol groups.

3.3. Discussion of silica reactivities in a cementitious environment

The properties of silica have to be considered for evaluating the main effects of silica on the hydration reactions of cement. The influence of the specific surface area is most obvious because it determines the interface between the solid silica and the pore solution. The comparison of the BET specific surface areas allows for the following reactivity ranking: pyrogenic silica > silica fume ≈ Stoeber particles.

Besides this purely geometric consideration, the intrinsic chemical reactivity of the silica surface is also important. Two different reaction sequences (paths I and II) should be observed:

Path I) silica dissolution (Eq. (4)) followed by the pozzolanic reaction (Eq. (8)),Path II) alite dissolution (Eq. (6)) and hydration (Eq. (5)), in which silica is not consumed but *C–S–H* phases nucleate on its surface (seeding effect).

The surface silanol group density (Section 3.1) is decisive for either path because it significantly affects the dissolution (previously discussed in Section 3.2) and the adsorption of ions which possibly affects the nucleation of *C–S–H* phases. Additionally, the total content of silanol groups of an entire particle needs to be taken in account for path I. As a consequence, Stoeber particles should be by far most reactive, followed by pyrogenic silica and the least reactive silica fume.

3.4. Investigations of UHPC pastes containing silica

3.4.1. Solid phases

The crystalline phases of UHPC paste were determined by in-situ XRD analysis 10 min and 1 h after mixing. Diffraction patterns for both reaction times were identical; therefore only the patterns after 1 h are shown in Fig. 7. Alite, belite, aluminate ferrite phase and ettringite (formed after Eq. (7)) are detected in all pastes. Gypsum is present in all samples including the dry CEM I powder (Fig. 8). Moreover, a significantly higher intensity of the (020) peak at 11.6° compared with the (021) reflection at 20.7° was observed in the UHPC pastes (Fig. 9). Such extraordinary relative intensities result from preferred orientation of crystals. The comparison with the intensity distribution for statistically oriented crystals given in PDF 033-0311 suggests a preferred gypsum orientation [010]. It is assumed that this orientation of the gypsum crystals results from a directed growth along the Kapton® foil. This formation of so-called secondary gypsum from previously dissolved bassanite was reported before for cementitious systems [13].

SEM images (Fig. 10) show that alite has straight edges and a smooth surface in all mortars 1 h after mixing. Silica particles and ettringite crystals prevail the microstructure. Gypsum is present in pastes with Stoeber particles and seems to overgrow the particles (Fig. 11). Its appearance

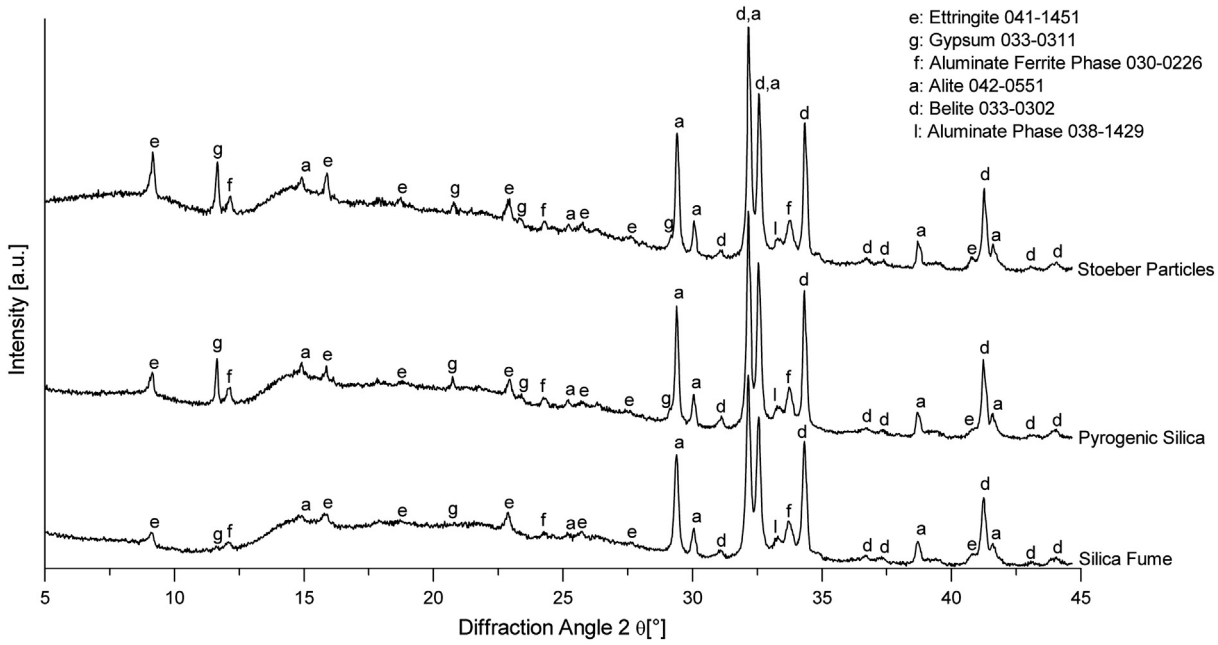

Fig. 7. XRD patterns of UHPC pastes at 1 h of hydration. Gypsum is present in all samples but a higher amount is detected in pastes with pyrogenic silica and Stoeber particles.

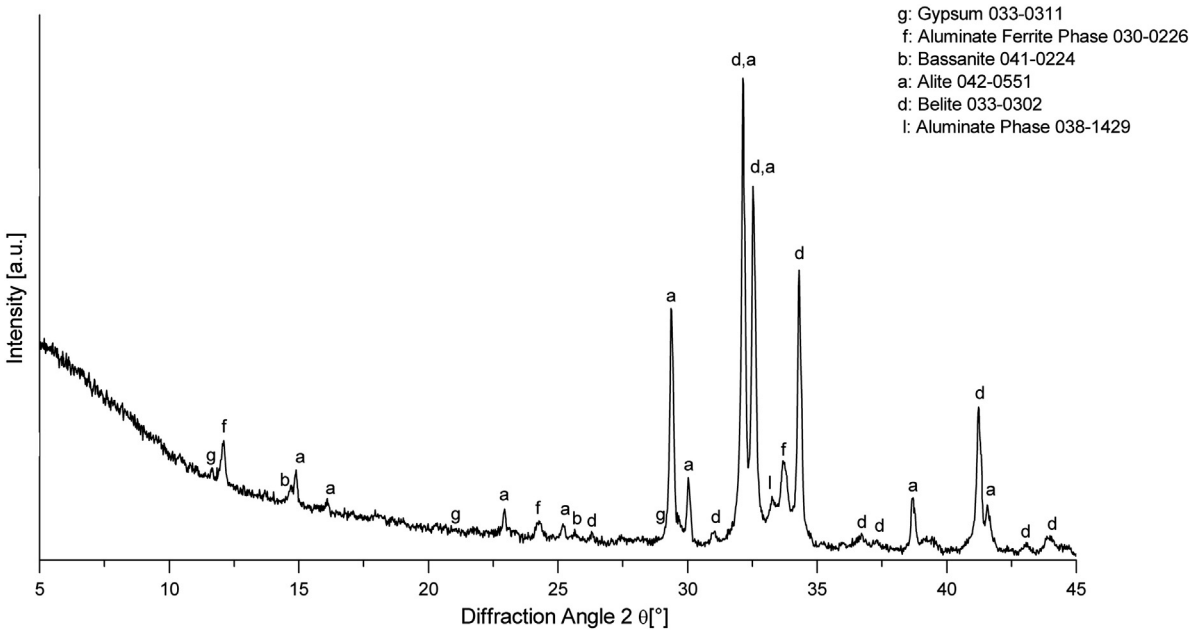

Fig. 8. XRD pattern of cement CEM I 52.5R HS/NA.

might be in accordance to the secondary growth indicated by the XRD results. *C–S–H* phases did not form, not even for the Stoeber particles which are assumed to be the most reactive silica in this study (see Section 3.3). This result corresponds to the observations made by Pfeiffer et al. [61] and Korpa et al. [28] who attributed the absence of *C–S–H* phases to the hydration retardation of the superplasticizer.

3.4.2. Pore solution

Na^+, K^+, Ca^{2+}, OH^-, SO_4^{2-} ions and silicate ions (e.g. $H_3SiO_4^-$) will be in the pore solution quickly after water addition to a cement [8,9]. They are formed from highly soluble alkali sulfates on the cement clinker surface (K_2SO_4, Na_2SO_4 and $Na_2SO_4 \cdot 3K_2SO_4$), the setting regulation agent (gypsum, bassanite and anhydrite), calcium oxide and the initial dissolution of clinker minerals (mostly alite and aluminate phase) [9]. Fig. 12 shows the analytic ion concentrations and pH values in pore solutions from the different UHPC pastes. The analytic results refer to total element concentrations nominated as: Na, K, Ca, sulfate and silicate. In detail, measured sulfur is most likely sulfate (SO_4^{2-}). The occurrence of different silicate species will be discussed later in this section.

Measured concentrations of Na, K and sulfate are below the maximum possible values (in mmol/l: Na = 300, K = 350 and sulfate = 1190, calculated from the analytical composition of the cement and w/c = 0.23 by mass) in all pore solutions. A certain amount of sodium and potassium is bound in the unhydrated clinker minerals. The sulfate concentration is diminished by the precipitation of ettringite [14] which was also detected in XRD. Ca and silicate may be dissolved from setting regulation agents, alite and silica. Measured pH values correspond to similar pastes [62].

Pastes containing pyrogenic silica show slightly lower concentrations for all measured elements than samples with silica fume. Remarkably, in the pore solution of pastes with Stoeber particles, K and Na concentrations drop by a factor of about 10^{-3}, sulfate by about 10^{-1}, whereas the silicate concentration increases. This lack in Na, K and sulfate is untypical for a cementitious paste. In addition, the concentration of Ca in pastes containing silica fume and Stoeber particles is significantly higher than the saturation concentration of Ca^{2+} ions for lime

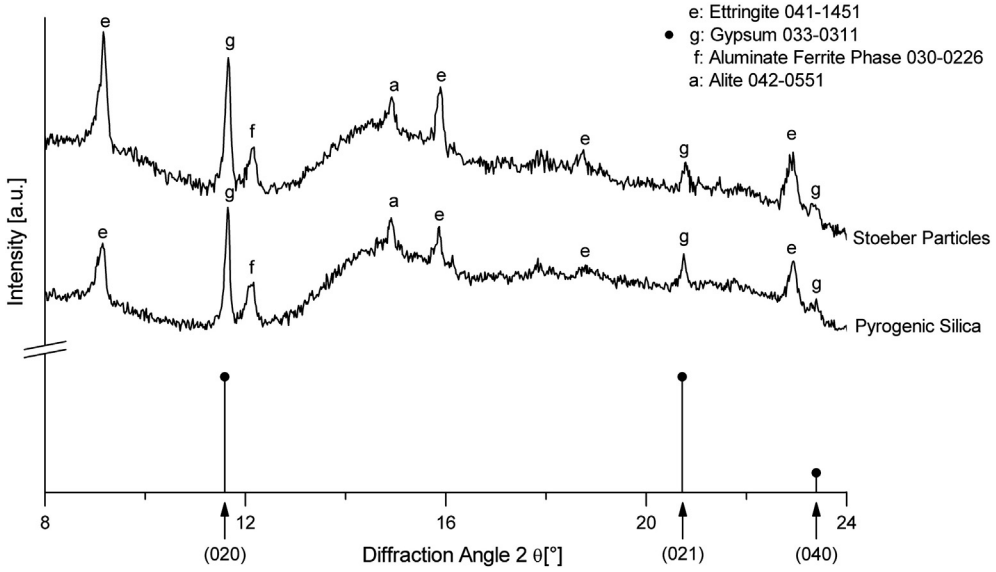

Fig. 9. Intensity of gypsum reflections of UHPC pastes with Stoeber particles and pyrogenic silica at 1 h of hydration. Enhanced intensity of (020) indicates preferred orientation of gypsum.

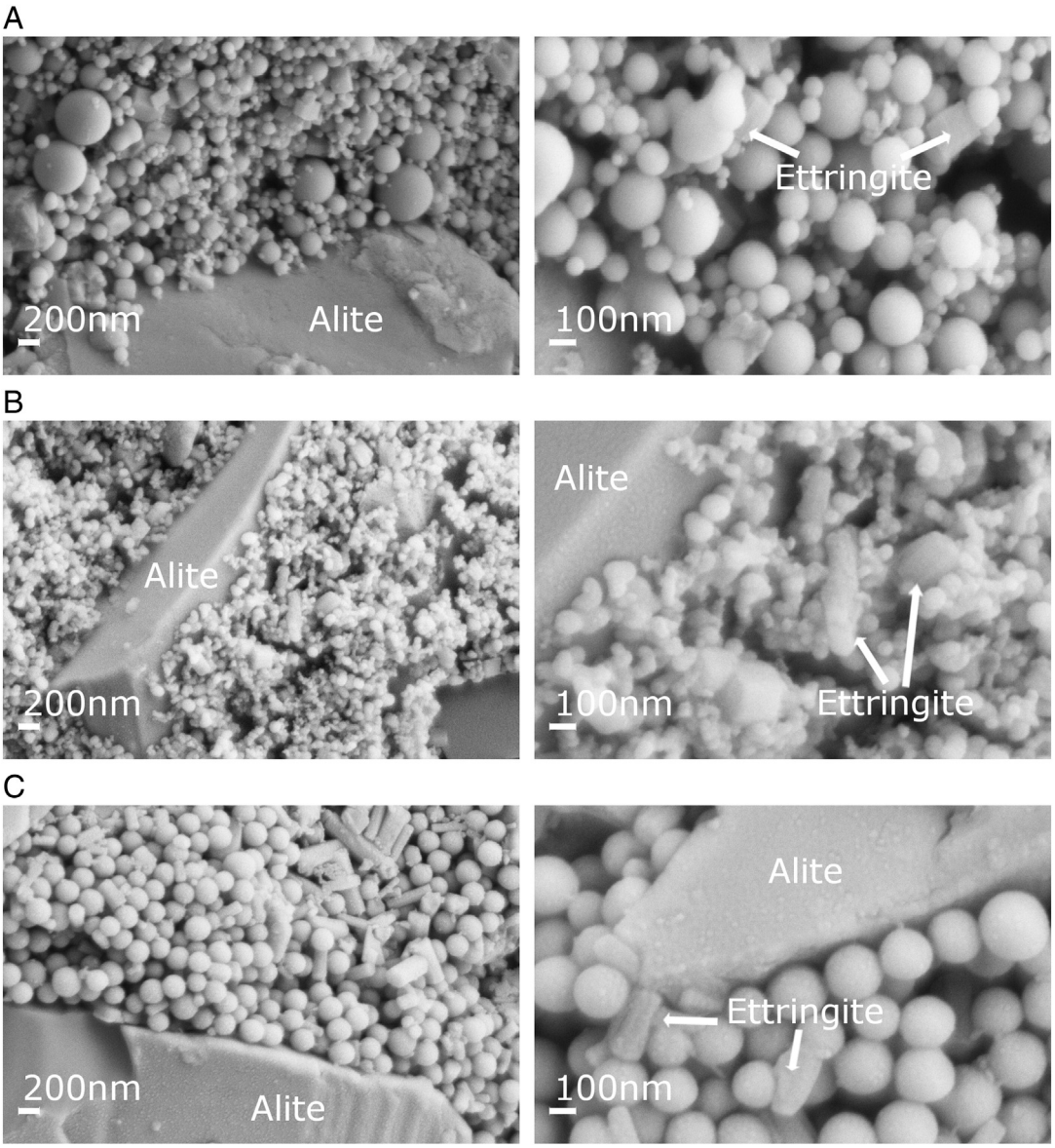

Fig. 10. SEM images of UHPC pastes after 1 h of hydration prepared by cryo-transfer technique (alite is confirmed by EDX, ettringite by morphology and in-situ XRD): A) silica fume, B) pyrogenic silica and C) Stoeber particles. The initial morphology of the particles is still visible. Silica particles are accompanied by ettringite.

(approx. 22 mmol/l). Different interactions at the interface between silica particles and the pore solution depending on the silica type may be assumed from the results and are discussed in the following.

For a deeper insight, the detailed processes at the silica surface have to be considered. As was already stated in the Introduction, simultaneously to the dissolution of silica in basic media (Eq. (4)), oligomeric silicate species are formed (Eq. (2)) [5,6]. The degree of this polymerization depends on the pH value and the concentration of ions in solution [5]. Na^+ and K^+ ions mostly lead to the formation of low molecular alkali silicate species (monomeric, dimeric or tetrameric

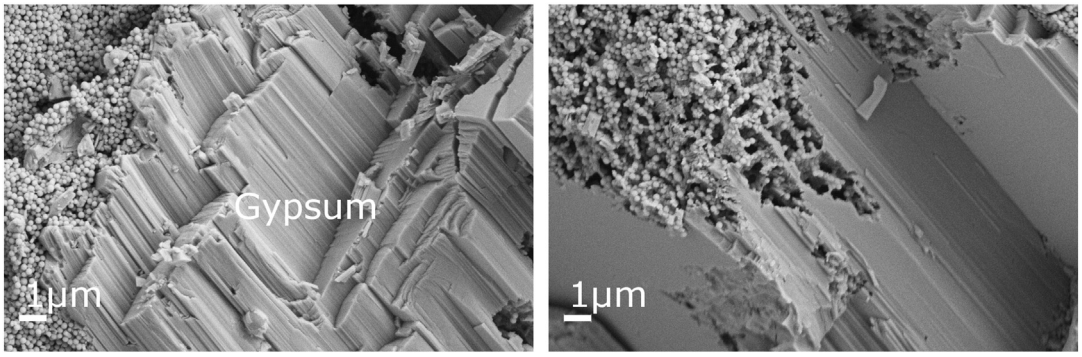

Fig. 11. SEM images of gypsum in paste containing Stoeber particles after 1 h of hydration prepared by cryo-transfer technique (gypsum is confirmed by in-situ XRD and EDX).

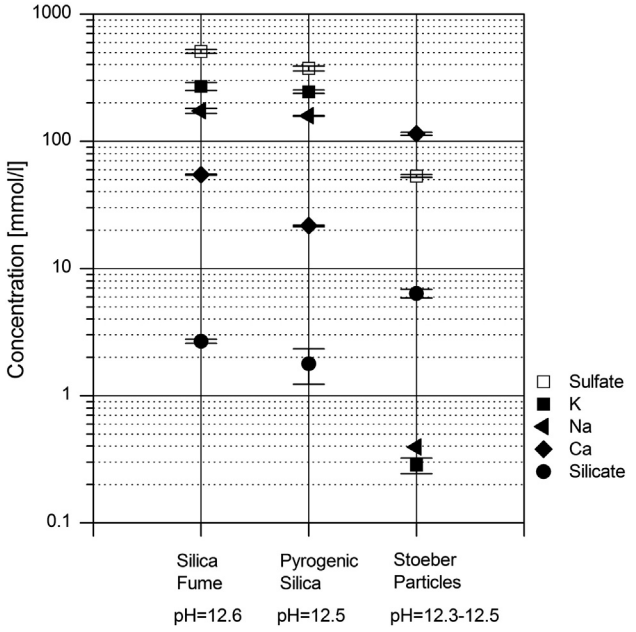

Fig. 12. Chemical composition of the pore solution from UHPC pastes (10 min after water addition, measurement error ± 2%). The average value and the standard deviation of three single measurements (silica fume and pyrogenic silica) and two single measurements (Stoeber particles, note that the second value for Na was measured 0 mmol/l) is shown. Stoeber particles significantly change the composition of the pore solution.

ions, e.g. $Si(OH)_2O_2M^-$, $Si_2(OH)_4O_3M^-$ and $Si_4(OH)_6O_6M^-$ with M = Na, K) [63,64], so-called alkali silicate oligomers like in water glass solutions. Eventually, they solidify to a gel by further condensation. Ca^{2+} ions can promote such a gel formation process [65], different mechanisms for this formation were proposed [65]. Bound sodium and potassium can also be replaced by calcium in the alkali silicate oligomers (so-called calcium alkali silicate oligomers) and possibly calcium silicate structures close to *C–S–H* phases are formed [66–68].

The analytic results of the total element concentrations of Na, K, Ca and silicate can be interpreted as follows taking into account those interactions of Na^+, K^+, Ca^{2+} and silicate ions. Although present in the pore solution after formation, alkali silicate oligomers and calcium alkali silicate oligomers do not contribute to the analytical results of Na, K, Ca and silicate. They may be removed by centrifugating together with clinker species and silica particles. As a consequence, analytical results for Na and K are understood as Na^+ and K^+ ions. The analytical concentration of Ca for pastes containing pyrogenic silica can be interpreted as Ca^{2+} ions because it is consistent with the saturation concentration of lime. For silica fume und Stoeber particles, analytical results for Ca above this saturation concentration might be explained by the formation of calcium silicate oligomers not being sedimented in the centrifugation residue. The analytical concentration of silicate being higher than in pastes containing silica fume supports this assumption.

Having the ranking of silica reactivities (Section 3.3) and the discussed interactions of Na^+, K^+ and Ca^{2+} ions in mind, the results of the pore solution analyses can be understood as a consequence of the silica reactivities. Na^+ and K^+ ions enter the pore solution immediately [9,15] and might be attracted to the negatively charged silica surface in the very early moment of mixing. They originate from alkali sulfates which are a relic from the cement production and cover the clinker minerals. Ca^{2+} ions enter the solution somewhat later. They are dissolved from calcium sulfates having a slower dissolution velocity than alkali sulfates [9]. After the dissolution of alkali sulfates, clinker minerals dissolve and provide additional Ca^{2+} ions. Na^+, K^+ and Ca^{2+} ions interact with dissolved silicate ions to alkali silicate oligomers, calcium alkali silicate oligomers and calcium silicate oligomers. The amount of dissolved silicate ions and oligomers depends on the silica reactivity which is postulated from the surface silanol group densities and total content of silanol groups (Section 3.3). Accordingly, it should be highest for Stoeber particles and lowest for silica fume. As a consequence, less alkali silicate oligomers and calcium alkali silicate oligomers are formed with silica fume and retain lower amounts of Ca, Na, K and silicate in the centrifugation residue (Fig. 12). This result agrees to the higher concentrations of those elements in the pore solutions in case of pastes containing silica fume.

The very low concentrations of Na and K in pastes containing Stoeber particles might indicate that alkali ions are almost completely bound in alkali silicate oligomers and removed by centrifugation. It is assumed, that the alkali silicate oligomers might even form a layer (amorphous gel phase) around the silica particles which is not detectable by cryo SEM or XRD. The still high concentration of silicate and Ca suggests that calcium silicate species are in the pore solution. The lower concentration of sulfates is in correspondence with the precipitation of secondary gypsum as observed by cryo SEM and XRD.

4. Conclusions

In this study, the effects of different types of silica (Stoeber particles, silica fume and pyrogenic silica) on the hydration of UHPC pastes were investigated within the first hour. Two different reaction sequences for silica (paths I and II) can be observed in a cementitious environment: either silica dissolves followed by a pozzolanic reaction (path I) or *C–S–H* phases from the hydration of alite nucleate at its surface (path II).

The silica reactivity was discussed considering different properties of silica. Surface silanol group densities, total contents of silanol groups and solubilities in alkaline suspensions indicate that Stoeber particles should be by far the most reactive, followed by pyrogenic silica and the less reactive silica fume. A different reactivity ranking is postulated (pyrogenic silica > silica fume ≈ Stoeber particles) if the specific surface area is considered which is twice as high for pyrogenic silica as for silica fume or Stoeber particles.

Silica reactions were further traced in UHPC pastes within the first hour of hydration by investigating the solid phases and the pore solution. The results give no indication for the reactivity ranking assumed from the specific surface area or for any reaction following path I or II. Instead, silica particles seem to attract cations (Na^+, K^+ and Ca^{2+}) from the pore solutions and form alkali silicate oligomers and calcium silicate oligomers. These oligomers might be held as a layer around the silica particles and form an aqueous, amorphous gel phase. The extent of the assumed oligomerization depends on the silica reactivity postulated from the surface silanol group density and the total content of silanol groups. Indeed, it seems to be high enough in pastes with Stoeber particles to bind almost all alkali ions in alkali silicate oligomers. The corresponding decline of alkali ions in the pore solution may have an impact on the subsequent processes because alkali ions accelerate the hydration of alite [69,70]. Therefore, the alite hydration in UHPC pastes containing Stoeber particles might not be as fast as in UHPC pastes containing other silica. Reaction path I seems to be more likely for Stoeber particles than for the less reactive pyrogenic silica and silica fume.

Further studies should investigate the effect of silica with different reactivities for an extended observation period to fully clarify the influence on the hydration (path I, II or both) and the resulting properties of UHPC.

Acknowledgments

The authors thank Johannes Prieschl for the Sears titration and XRD measurements, Kirsten Langguth for her support in taking SEM images, Rüdiger Bertermann for measuring and quantifying ^{29}Si NMR, Jürgen Göske for in-situ XRD measurements, Susanne Winter for cryo SEM preparation and imaging and Werner Hopp for ICP measurements. Professor Josef Breu is acknowledged for his advices and discussions

throughout the implementation of this work. Also, many thanks go to Joachim Krakehl and Holger Kletti for fruitful discussions. The research was funded by the Elite Network of Bavaria in the International Graduate School 'Structure, Reactivity and Properties of Oxide Materials' and partially by the German Federal Ministry of Education and Research in the project 'Chemically Bonded Ceramics by Nanotechnological Improvements of Structure (03X0067E)'.

References

[1] A.E. Naaman, K. Wille, The path to ultra-high performance fiber reinforced concrete (UHP-FRC): five decades of progress, in: M. Schmidt, E. Fehling, C. Glotzbach, et al., (Eds.), Proceedings of 3rd Hipermat: International Symposium on UHPC and Nanotechnology for High Performance Construction Materials, Kassel University Press, Kassel, 2012, pp. 3–16.
[2] E. Fehling, M. Schmidt, T. Teichmann, et al., Entwicklung, Dauerhaftigkeit und Berechnung Ultrahochfester Betone (UHPC), Forschungsbericht DFG FE 497/1-1, Kassel University Press, Kassel, 2005.
[3] Verein Deutscher Zementwerke, Reaktive Zusatzstoffe (Typ II), Zement-Taschenbuch, Verlag Bau + Technik GmbH, Düsseldorf, 2008.
[4] M. Schmidt, Nanotechnologie: Neue Ansätze für die Entwicklung von Hochleistungsbindemitteln und -betonen, in: J. Stark (Ed.), Proceedings of 17th Ibausil: Internationale Baustofftagung, Weimar, 2009, 2009.
[5] R.K. Iler, The Chemistry of Silica, John Wiley & Sons, Inc., New York, 1978.
[6] M. Fertani-Gmati, M. Jemal, Thermochemistry and kinetics of silica dissolution in NaOH aqueous solution, Thermochim. Acta 513 (2011) 43–48.
[7] J.W. Bullard, H.M. Jennings, R.A. Livingston, et al., Mechanisms of cement hydration, Cem. Concr. Res. 41 (2011) 1208–1223.
[8] H.F.W. Taylor, Cement Chemistry, 2nd ed. Thomas Telford Publishing, London, 1997.
[9] I. Odler, Hydration, setting and hardening of Portland cement, in: P.C. Hewlett (Ed.), Lea's Chemistry of Cement and Concrete, Elsevier Ltd., London, 2004, pp. 241–297.
[10] S. Mindess, J.F. Young, Concrete, Prentice Hall, Englewood Cliffs, 1981.
[11] K.L. Scrivener, A. Nonat, Hydration of cementitious materials, present and future, Cem. Concr. Res. 41 (2011) 651–665.
[12] F.M. Lea, The Chemistry of Cement and Concrete, 3rd ed. Edward Arnold, Glasgow, 1970.
[13] M. Merlini, G. Artioli, T. Cerulli, et al., Tricalcium aluminate hydration in additivated systems. A crystallographic study by SR-XRPD, Cem. Concr. Res. 38 (2008) 477–486.
[14] C. Hesse, F. Goetz-Neunhoeffer, J. Neubauer, A new approach in quantitative in-situ XRD of cement pastes: correlation of heat flow curves with early hydration reactions, Cem. Concr. Res. 41 (2011) 123–128.
[15] B. Lothenbach, F. Winnefeld, Thermodynamic modelling of the hydration of Portland cement, Cem. Concr. Res. 36 (2006) 209–226.
[16] J. Björnström, A. Martinelli, A. Matic, et al., Accelerating effects of colloidal nano-silica for beneficial calcium–silicate–hydrate formation in cement, Chem. Phys. Lett. 392 (2004) 242–248.
[17] B. Jo, C. Kim, G. Tae, et al., Characteristics of cement mortar with nano-SiO_2 particles, Constr. Build. Mater. 21 (2007) 1351–1355.
[18] B. Lothenbach, K. Scrivener, R.D. Hooton, Supplementary cementitious materials, Cem. Concr. Res. 41 (2011) 1244–1256.
[19] L. Senff, J.A. Labrincha, V.M. Ferreira, et al., Effect of nano-silica on rheology and fresh properties of cement pastes and mortars, Constr. Build. Mater. 23 (2009) 2487–2491.
[20] L. Senff, D. Hotza, W.L. Repette, et al., Mortars with nano-SiO_2 and micro-SiO_2 investigated by experimental design, Constr. Build. Mater. 24 (2010) 1432–1437.
[21] J.Y. Shih, T.P. Chang, T.C. Hsiao, Effect of nanosilica on characterization of Portland cement composite, Mater. Sci. Eng. A 424 (2006) 266–274.
[22] T. Oertel, F. Hutter, R. Tänzer, et al., Primary particle size and agglomerate size effects of amorphous silica in ultra-high performance concrete, Cem. Concr. Compos. 37 (2013) 61–67.
[23] H.W. Krauss, H. Budelmann, Hydration kinetics of cement paste with very fine inert mineral additives, Proceedings RILEM 79, Hong Kong, 2011, pp. 58–65.
[24] H.W. Krauss, H. Budelmann, Agglomeration und räumliche Anordnung von Feinstoffpartikeln in Zementleim - physikalische Mechanismen und Einfluss auf die Hydratation, in: F. Winnefeld, F. Deschner (Eds.), Proceedings of Tagung Bauchemie, GDCH- Fachgruppe Bauchemie, Dübendorf, 2012, pp. 35–42.
[25] Y. Qing, Z. Zenan, K. Deyu, et al., Influence of nano-SiO_2 addition on properties of hardened cement paste as compared with silica fume, Constr. Build. Mater. 21 (2007) 439–545.
[26] A. Korpa, T. Kowald, R. Trettin, Hydration behaviour, structure and morphology of hydration phases in advanced cement-based systems containing micro and nanoscale pozzolanic additives, Cem. Concr. Res. 38 (2008) 955–962.
[27] A. Korpa, R. Trettin, K.G. Böttger, et al., Pozzolanic reactivity of nanoscale pyrogene oxides and their strength contribution in cement-based systems, Adv. Cem. Res. 20 (2008) 35–46.
[28] A. Korpa, T. Kowald, R. Trettin, Phase development in normal and ultra high performance cementitious systems by quantitative X-ray analysis and thermoanalytical methods, Cem. Concr. Res. 39 (2009) 69–76.
[29] J.J. Thomas, H.M. Jennings, J.J. Chen, Influence of nucleation seeding on the hydration mechanisms of tricalcium silicate and cement, J. Phys. Chem. C 113 (2009) 4327–4334.
[30] S.A. Greenberg, Reaction between silica and calcium hydroxide solutions. I. kinetics in the temperature range 30 to 85 °C, J. Phys. Chem. 65 (1961) 12–16.
[31] N.Y. Mostafa, P.W. Brown, Heat of hydration of high reactive pozzolans in blended cements: isothermal conduction calorimetry, Thermochim. Acta 435 (2005) 162–167.
[32] A.G. Degussa, Technical Bulletin Fine Particles, 112006.
[33] W. Stoeber, A. Fink, Controlled growth of monodisperse silica spheres in the micron size range, J. Colloid Interface Sci. 26 (1968) 62–69.
[34] H.E. Bergna, Chapter 3: colloidal chemistry of silica: an overview, in: H.E. Bergna, W.O. Roberts (Eds.), Colloidal Silica: Fundamentals and Applications, CRC Press Taylor & Francis Group, Boca Raton, 2006, pp. 9–35.
[35] T.I. Suratwala, M.L. Hanna, E.L. Miller, et al., Surface chemistry and trimethylsilyl functionalization of Stoeber silica sols, J. Non-Cryst. Solids 316 (2003) 349–363.
[36] C.J. Brinker, G.W. Scherer, Sol–gel Science: The Physics and Chemistry of Sol–gel Processing, Academic Press, San Diego, 1990.
[37] H.E. Bergna, Chapter 2: the language of colloidal science and silica chemistry, in: H.E. Bergna, W.O. Roberts (Eds.), Colloidal Silica: Fundamentals and Applications, CRC Press Taylor & Francis Group, Boca Raton, 2006, pp. 9–35.
[38] V.D. Khavryuchenko, O.V. Khavryuchenko, V.V. Lisnyak, Formation of pyrogenic silica: spectroscopic and quantum chemical insight, Crit. Rev. Solid State Mater. Sci. 36 (2011) 47–65.
[39] Fédération Internationale de la Précontrainte, Condensed Silica Fume in Concrete — FIP State of Art Report, Thomas Telford Publishing, London, 1988.
[40] S. Fröhlich, M. Schmidt, Influences on repeatability and reproducibility of testing methods for fresh UHPC, in: M. Schmidt, E. Fehling, C. Glotzbach, et al., (Eds.), Proceedings of 3rd Hipermat: International Symposium on UHPC and Nanotechnology for High Performance Construction Materials, Kassel University Press, Kassel, 2012, pp. 225–232.
[41] G.W. Sears, Determination of specific surface area of colloidal silica by titration with sodium hydroxide, Anal. Chem. 28 (1956) 1981–1983.
[42] J. Göske, S. Winter, H. Pöllmann, et al., Hydraulische Reaktionen des Zements in Mörtel bei verschiedenen Parametern, Beton- Stahlbetonbau 105 (2010) 521–528.
[43] M. Fylak, J. Göske, W. Kachler, et al., Cryotransfer scanning electron microscopy for the study of cementitious systems, Microsc. Anal. 20 (2006) 9–12.
[44] S. Diamond, S. Sahu, Densified silica fume: particle sizes and dispersion in concrete, Mater. Struct. 39 (2006) 849–859.
[45] G. Orts-Gil, K. Natte, D. Drescher, et al., Characterisation of silica nanoparticles prior to in vitro studies: from primary particles to agglomerates, J. Nanopart. Res. 13 (2011) 1593–1604.
[46] C. Despas, A. Walcarius, J. Bessière, Influence of the base size and strength on the acidic properties of silica gel and monodispersed silica beads: interest of impedance measurements for the in situ monitoring of the ionization process, Langmuir 15 (1999) 3186–3196.
[47] M. Kobayashi, M. Skarba, P. Galletto, et al., Effects of heat treatment on the aggregation and charging of Stöber-type silica, J. Colloid Interface Sci. 292 (2005) 139–147.
[48] J.W. Perram, Structure of the double layer at the oxide/water interface, J. Chem. Soc. Faraday Trans. 2 (69) (1973) 993–1003.
[49] Q. Wan, C. Ramsey, G. Baran, Thermal pretreatment of silica composite filler materials, J. Therm. Anal. Calorim. 99 (2010) 237–243.
[50] D.E. Yates, T.W. Healy, The structure of the silica/electrolyte interface, J. Colloid Interface Sci. 55 (1976) 9–19.
[51] Ullmann's Encyclopedia of Industrial Chemistry, Colloidal Silica, 6th ed. Whiley-VCH, 2003.
[52] J.D. Rimstidt, H.L. Barnes, The kinetics of silica–water reactions, Geochim. Cosmochim. Acta 44 (1980) 1683–1699.
[53] G. Berger, E. Cadore, J. Schott, et al., Dissolution rate of quartz in lead and sodium electrolyte solutions between 25 and 300 °C: effect of the nature of surface complexes and reaction affinity, Geochim. Cosmochim. Acta 58 (1994) 541–551.
[54] J.D. Rimer, O. Trofymluk, A. Navrotsky, et al., Kinetic and thermodynamic studies of silica nanoparticle dissolution, Chem. Mater. 19 (2007) 4189–4197.
[55] W. Tscharnuter, Photon correlation spectroscopy in particle sizing, in: R.A. Meyers (Ed.), Encyclopedia of Analytical Chemistry, John Wiley & Sons Ltd., Chichester, 2000, pp. 5469–5485.
[56] B. Derjaguin, L. Landau, Theory of the stability of strongly charged lyophobic sols and of the adhesion of strongly charged particles in solutions of electrolytes, Acta Phys. Chem. URSS 14 (1941) 633–662.
[57] E.J.W. Verwey, J.T.G. Overbeek, Theory of the Stability of Lyophobic Colloids, Elsevier Publishing Company, New York, 1948.
[58] T.W. Healy, Chapter 20: stability of aqueous silica sols, in: H.E. Bergna, W.O. Roberts (Eds.), Colloidal Silica: Fundamentals and Applications, CRC Press Taylor & Francis Group, Boca Raton, 2006.
[59] E.J.W. Verwey, Theory of the stability of lyophobic colloids, J. Phys. Chem. 51 (1947) 631–636.
[60] S. Jenkins, S.R. Kirk, M. Persson, et al., The role of hydrogen bonding in nanocolloidal amorphous silica particles in electrolyte solutions, J. Colloid Interface Sci. (2009) 351–361.
[61] C. Pfeifer, B. Möser, J. Stark, Hydration, phase and microstructure development of ultra-high performance concrete, ZKG Int. 63 (2010) 71–79.
[62] C. Schröfl, Omega-Methoxypoly(ethylenoxid)-Methacrylsäureester-co-Methacrylsäure-co-Methallylsulfonsäure-Polycarboxylate als Fließmittel für ultra-hochfesten Beton: Synthese, Wirkmechanismus und Untersuchungen zum Synergismus von selektiv adsorbierenden Polymergemischen, (Doctoral thesis) Technische Universität München, München, 2010.
[63] M. Tanaka, K. Takahashi, The identification of chemical species of silica in sodium hydroxide, potassium hydroxide and sodium chloride solutions by FAB-MS, Anal. Sci. 15 (1999) 1241–1250.
[64] A.M. Berninger, Mikrostrukturelle Eigenschaften von Quarz als Bestandteil spät reagierender, alkaliempfindlicher Zuschläge, (doctoral thesis) Bauhaus University, Weimar, 2004.

[65] F. Gaboriaud, A. Nonat, D. Chaumont, Aggregation and gel formation in basic silico-calco-alkaline solutions studied: a SAXS, SANS, and ELS study, J. Phys. Chem. B 103 (1999) 5775–5781.
[66] A. Leemann, G. Le Saout, F. Winnefeld, et al., Alkali–silica reaction: the influence of calcium on silica dissolution and the formation of reaction products, J. Am. Ceram. Soc. 94 (2011) 1243–1249.
[67] D.E. Macphee, K. Luke, F.P. Glasser, et al., Solubility and aging of calcium silicate hydrates in alkaline solutions at 25 °C, J. Am. Ceram. Soc. 72 (1989) 646–654.
[68] L.H. Allen, E. Matijevic, Stability of colloidal silica: I. Effect of simple electrolytes, J. Colloid Interface Sci. 31 (1969) 286–296.
[69] A. Kumar, G. Sant, C. Patapy, et al., The influence of sodium and potassium hydroxide on alite hydration: experiments and simulations, Cem. Concr. Res. 42 (2012) 1513–1523.
[70] V. Morin, S. Garrault, F. Begarin, et al., The influence of an ion-exchange resin on the kinetics of hydration of tricalcium silicate, Cem. Concr. Res. 40 (2010) 1459–1464.